

A Novel Preparation and Vapour Phase Modification of 2D-open Channel Bio-adsorbent Via ATRP for Uranium Separation

Mudasir Ahmad¹, Jianquan Ren¹, Tao Xiu¹, Mehraj-ud-din Naik², Qiuyu Zhang¹, and Baoliang Zhang¹

¹Northwestern Polytechnical University

²Jazan University

February 22, 2024

Abstract

An economical and highly uranium extraction from seawater remains a crucial task for energy sources and environmental safety. Aiming for improving mass transfer rate of uranium adsorption from seawater, a new synthetic strategy was adopted for the fabrication of 2D-open channel microporous bio-adsorbent for uranium extraction from seawater. Herein, the in-situ ATRP grafting approach was adopted to graft divinylbenzene, polyacrylonitrile onto the surfaces of microporous frameworks via the vapour phase method. The post-synthetic functionalization was carried out by hydrothermal method, where amidoxime groups are structure-directing agents to trap uranium. Further, amidoxime groups not only enhanced hydrophilicity but also adjusts adsorbents pKa. AO-Fc faces minimum interference of competing ions and achieves a high uranium adsorption capacity of 8.57 ± 0.02 and 409 ± 1 mg/g in seawater and simulated solution. Despite its stable structure, AO-Fc exhibits a long life span and negligible weight loss revealed AO-Fc could be applied as a potential adsorbent for radionuclide.

A Novel Preparation and Vapour Phase Modification of 2D-open Channel Bio-adsorbent Via ATRP for Uranium Separation

Mudasir Ahmad ^{a, b}, Jianquan Ren ^a, Tao Xiu ^a, Mehraj-ud-din Naik ^c, Qiuyu Zhang ^{a, b}, Baoliang Zhang ^{a, d}, ¹¹Corresponding author, Northwestern Polytechnical University, Youyi Road 127#, Xi'an (710072), China. Email: blzhang@nwpu.edu.cn

^a School of Chemistry and Chemical Engineering, Northwestern Polytechnical University, Xian, China, 710072.

^b Xian Key laboratory of Functional Organic porous materials, Northwestern Polytechnical University, China, 710129.

^c Department of Chemical Engineering, College of Engineering, Jazan University, Jazan 45142, Kingdom of Saudi Arabia.

^d Shaanxi Engineering and Research Center for Functional Polymers on Adsorption and Separation, Sunresins New Materials Co. Ltd., Xi'an, 710072, China.

Abstract: An economical and highly uranium extraction from seawater remains a crucial task for energy sources and environmental safety. Aiming for improving mass transfer rate of uranium adsorption from seawater, a new synthetic strategy was adopted for the fabrication of 2D-open channel microporous bio-adsorbent for uranium extraction from seawater. Herein, the in-situ ATRP grafting approach was adopted to graft divinylbenzene, polyacrylonitrile onto the surfaces of microporous frameworks via the vapour phase method. The post-synthetic functionalization was carried out by hydrothermal method, where amidoxime groups are

structure-directing agents to trap uranium. Further, amidoxime groups not only enhanced hydrophilicity but also adjusts adsorbents pKa. AO-Fc faces minimum interference of competing ions and achieves a high uranium adsorption capacity of 8.57 ± 0.02 and 409 ± 1 mg/g in seawater and simulated solution. Despite its stable structure, AO-Fc exhibits a long life span and negligible weight loss revealed AO-Fc could be applied as a potential adsorbent for radionuclide.

Keywords: Microporous bioadsorbent; 2D-open channel; vapor-phase modification; ATRP; uranium

Introduction

A rapid increase in energy demands has given rise to energy shortage, nuclear energy with the advantage of low carbon emission play an important role in sustainable energy source^{1,2}. Uranium plays a key role in nuclear energy sources, therefore its extraction is very important for continuous energy supply³⁻⁵. However, it is estimated uranium in the terrestrial ores is limited and at the current usage, the terrestrial resources might be ended at the end of the current century⁶. Comparatively, it is estimated 4.5 billion tons of uranium in seawater, which is a thousand times higher than terrestrial ores⁷⁻⁹. Therefore, a new strategy needs to develop to extract efficient uranium from seawater to fill the energy gap, environmental protection and sustainable development. However, the presence of competing ions, low uranium concentration (3.3 ppb) and high-cost synthetic preparation hinder the development of materials for the extraction of uranium from natural seawater¹⁰⁻¹⁴. Various materials such as porous organic polymers (POPs)^{15,16}, covalent organic frameworks (COFs)¹⁷⁻¹⁹, porous aromatic frameworks (PAFs)^{3,20}, metal-organic frameworks (MOFs)^{21,22} and biopolymers²³⁻²⁵ have been used for the extraction of uranium from seawater. Among all of them, amidoxime-modified adsorbents are promising with the advantage of high selectivity towards uranium in seawater²⁶⁻²⁹. However, the development of most of the material is either expensive, difficult to synthesize, poor stability and low uranium adsorption efficiency in seawater. Recently, efforts have been devoted to developing advanced materials via simple and facile methods from inexpensive raw materials with ample uranium adsorption capacity.

Charcoal-based materials are highly interested due to their low cost, porous structure, and environmentally friendly nature^{1,30-32}. Recently, amidoxime modified hollow fibers were used for uranium adsorption³³. Zhou et al. reported 1D porous adsorbent from wood waste for adsorption of polycyclic aromatic hydrocarbons³⁴. Liao et al. reported pig manure-based biochar for uranium extraction³⁵. Wang et al. reported 1D amidoxime modified bamboo charcoal for uranium extraction from seawater³⁶. The drawbacks of already available amidoxime modified charcoal-based adsorbents for uranium extraction are as follows; (i) Regarding the analysis and reporting the adsorption results, the experimental adsorption uncertainty is currently missing, (ii) the preparation method is difficult or low functionalization yield and or perform well under inert atmospheres, (iii) use of high cost solvents for the preparation and purification process and (iv) requirement of typical experimental procedure with critical conditions. In this work we could sort out these problems as well by carrying a simple method by carbonization process in vacuum and subsequent vapor phase modification via ATRP to obtain highly functionalized ultra-porous material. Then after the post-synthetic modification was carried to convert nitrile groups into amidoxime functional groups onto the surface of 2D channels by hydrothermal method. The uncertainty in uranium adsorption experiment was measurement by using classic concepts of error propagation.

2. Experimental section

Materials

Wood (Chinese fir) was obtained from Heilongjiang province, China. Acrylonitrile and azobisisobutyronitrile, uranyl nitrate, sodium chloride, and sodium bicarbonate were purchased from Changzhou Qidi Chemical Co., Ltd. Divinylbenzene, hydroxylamine hydrochloride. NaOH and ethanol were obtained from Hubei Jusheng Technology Co., Ltd. The double-distilled water was obtained from a laboratory filtration plant.

Preparation of nitrile functionalized charcoal (CN-Fc)

Wood (Chinese fir, 5 g) was used as a starting material for the preparation of charcoal in this study. A simple

carbonization process was carried out at 600 °C with a heating rate of 10°C/min in a vacuum for 3 h. Then, acrylonitrile (5 g) and azobisisobutyronitrile (0.1 g) and charcoal (0.5 g) were added to a beaker for 30 min. The samples were taken and kept in a glass tube which was 100 mm in length and 30 mm in diameter and the tube was kept in an oven at 180 °C for 5 h. To achieve higher nitrile content, 0.8 g of divinylbenzene was added in a solution of acrylonitrile (5 g), azobisisobutyronitrile (0.1 g) under the same set of reaction conditions mentioned above. The obtained products were denoted as CN-Fc and CN-Fc1, where 1 represents an absence of divinylbenzene in the reaction system.

Preparation of amidoxime modified charcoal (AO-Fc)

The amidoximation process was carried out by adopting a previous method with small modifications³⁶. Hydroxylamine hydrochloride (0.48 g) and NaOH (0.25 g) were dissolved in ethanol (15 mL) using an ultrasonicator for 15 min. In the meantime, CN-Fc (0.48 g) and the prepared solution were transferred in 50 mL Teflon lined autoclave, which was kept at 70 °C for 24 h. After cooling, the product was washed with distilled water several times, dried in a vacuum at 60 °C for 12 h and the obtained product was AO-Fc.

Characterization

The morphology was analyzed by using FEI Verios G4 scanning electron microscopy (SEM) and the energy dispersive spectrum (EDS) was carried out by using a Bruker Everhart-Thornley Detector. For chemical structure determination, FTIR (Bruker TENSOR 27 spectrophotometer) and Powder X-ray diffraction (Thermo Scientific 7000 diffractometer) were used. The hydrophilicity was determined using a contact angle analyzer. The thermal stability was analyzed using a Mettler Toledo Thermogravimetric analyzer with a heating rate of 10 °C/min under a nitrogen atmosphere in a temperature range of 40-800°C. The X-ray photoelectron spectrum was obtained by using Kratos Axis Ultra DLD analyzer and the peak fitting of performed using XPS peak fitting program version 4.1. Nitrogen adsorption-desorption was carried out using the Tristar3020 Micromeritics analyzer.

Uranium extraction from natural seawater

A homemade experimental setup (Figure S1) was developed to investigate the adsorption capacity of the AO-Fc in simulated seawater and natural seawater. The simulated seawater was obtained by dissolving uranyl nitrate (0.017 g), sodium chloride (25 g), and sodium bicarbonate (0.193) in distilled water and further, diluted to obtain different uranium initial concentrations of 0.003 to 1 mg/L. The influence of pH on uranium adsorption, contact time, initial uranium concentration, and the presence of various competing ions was investigated. The pH of the solution was set by adding the required quantity of 0.1 M HNO₃ and NaOH solution. For each experiment, the adsorbent was packed in a syringe to hold it and let the penetration of the adsorption solution. The solution was pumped using a lincolin pump with a flow speed of 150 mL/min at room temperature.

For real seawater, we have packed adsorbent (7 mg) in a syringe to hold the adsorbent. A real seawater 20 L was obtained from the South China Sea near Shandong province. The adsorption capacities of metal ions were estimated by collecting a 5 mL sample every day for 39 days. The metal ions concentration was determined by using an inductively coupled plasma emission spectrometer (ICPS-MS, 6300, ThermoFisher Scientific). The uranium adsorption capacity (q_e mg/g) and adsorption efficiency (Ads %) can be written as shown in equation 1 and 2.

$$q_e = \frac{(C_o - C_e)}{m} \times V \quad (1)$$

$$Ads \% = \frac{(C_o - C_e)}{C_o} \times 100 \quad (2)$$

Where q_e is the equilibrium adsorption capacity weight per unit mass (mg/g) C_o and C_e represent initial concentration and equilibrium concentration weight per unit volume (mg/L), V is a volume of solution in liters (L) and mass of adsorbent in grams (g).

To determine the adsorbent regeneration, the adsorbent (7 mg) was eluted by using a 21 mL elution solution (Na₂CO₃, 1 M and H₂O₂, 0.1 M) at room temperature for 1 hour to remove the adsorbed uranium from the

adsorbent surface. The elution efficiency can be expressed as shown in equation 3.

$$\frac{C_{el} \times V_{el}}{(C_a - C_o) \times V_a} \times 100(3)$$

Where C_{el} denotes elution concentration (mg/L), V_{el} is the elution volume (L), C_a represents uranium concentration in seawater after adsorption (mg/L), C_o initial concentration of metal ions (mg/L) and V_a volume of seawater used for adsorption (L).

Results and discussion 3.1 Adsorbent synthesis and characterization

To achieve efficient uranium extraction from seawater, it is critical to develop highly porous adsorbent material with efficient stability and selectivity toward uranium in natural seawater. As shown in Figure 1, two different approaches have been adopted to functionalize the virgin fir-charcoal (Fc) and subsequent post-synthetic functionalization was followed to enhance uranium adsorption of targeted adsorbent in seawater. Firstly, Fc undergoes vapor phase modification with acrylonitrile and azobisisobutyronitrile as an initiator to obtain nitrile functionalized material (CN-Fc) via ATRP. Secondly, the functionalization was enhanced by adding divinylbenzene as an additional component under the same set of experimental conditions to yield CN-Fc. In post-synthetic functionalization under alkaline conditions, nitrile groups were converted into amidoxime groups via a hydrothermal process.

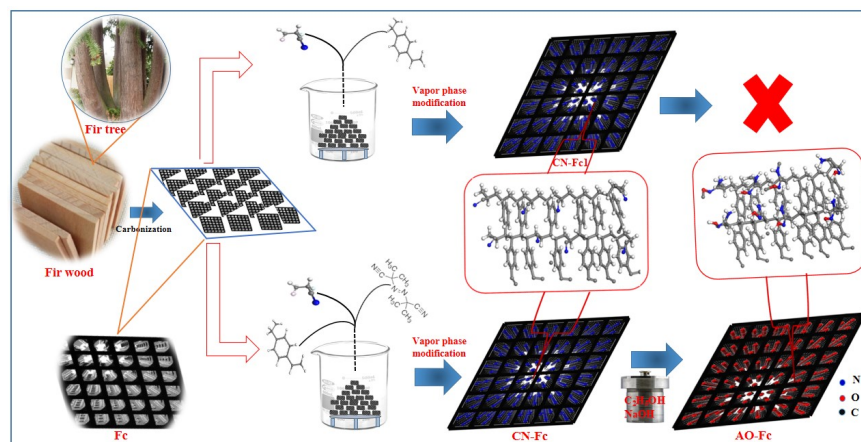


Figure 1 Step by step preparation of AO-Fc adsorbent material

The chemical structure was confirmed by FTIR and XPS analysis. The FTIR spectra of Fc, CN-Fc, CN-Fc1 and AO-Fc were shown in Figure 2a. All spectra have similar shapes in the vibration band of carbonaceous material and a peak at 3500-3700 cm^{-1} was observed due to the presence of OH groups^{36,37}. Afterward, Fc was modified with the aid of azobisisobutyronitrile and divinylbenzene to yield CN-Fc. On comparing the FTIR spectrum of CN-Fc and CN-Fc1, the peaks in the spectra at 2242 cm^{-1} were assigned to C[?]N and high peak intensity witnessed the higher payload of nitrile groups were seen on CN-Fc than CN-Fc1³⁸. The post-synthetic functionalization further converted C[?]N groups into C=N, C-N and N-O confirmed by respective peaks at 1638 cm^{-1} , 1380 cm^{-1} and 928 cm^{-1} respectively, indicating the presence of amidoxime groups on the surface of Fc³⁹. The presence of amidoxime groups were further investigated by XPS analysis (Figure 2b-d); in C 1s high-resolution spectra of AO-Fc (Figure 2b) showed two peaks at 284.45 eV and 285.5 eV assigned to C-N and C=N; in N 1s spectrum of AO-Fc (Figure 2c) showed two peaks at 400.05 eV and 398.40 eV assigned to N-H and C=N respectively³⁶, and the O 1s spectra of AO-Fc (Figure 2d) showed two peaks at 532.5 eV and 531.9 eV assigned to C(NH₂)-N-OH and O-H groups respectively⁴⁰. The powder XRD patterns of Fc, CN-Fc and AO-Fc were shown in Figure 2e. The XRD patterns showed peaks around 16.2° which can be indexed (101) plane and confirmed the amorphous nature of the material⁴¹. Furthermore, a broad

peak was seen at around 25° and a small peak nearly 43° , which can be indexed (0002), (1010/1011) plane of graphite and are consistent with the presence of amorphous carbon⁴². The contribution of amidoxime groups on the surface of AO-Fc was calculated by carrying thermogravimetric analysis. Compared with Fc, a significant weight loss (80 %) was observed in AO-Fc in the temperature range of 300°C to 550°C (Figure 2f). The higher weight loss in AO-Fc was due to the large amount organic groups were thermally decayed, which confirmed the weight contribution of amidoxime groups taken to 80 % of the weight loss of AO-Fc.

Figure 2 FTIR spectra (a), high-resolution XPS spectra of C 1s (b) N 1s (c) and O 1s (d), powder XRD pattern (e), and TGA curves (f)

SEM morphology of the vertical and horizontal cross-section of Fc, CN-Fc, CN-Fc1, and AO-Fc were shown in Figure 3. The structure of Fc was seen with two-dimensional rectangular two open-end vessels arranged in a proper array with a breadth of $28.6\ \mu\text{m}$ (Figure S2a) and height of $18.3\ \mu\text{m}$ (Figure 3abc) and (Figure S2b). SEM images of CN-Fc and CN-Fc1 were not changed obviously after chemical modification (Figure 3de). However, high magnified SEM images showed the rectangular walls were covered with small structures that confirmed the presence of chemical groups. Comparison to Fc, AO-Fc SEM images showed thick wall rectangular vessels (high magnified image) (Figure 3f) without any collapse or damage with a height and breadth of approximately $27.02\ \mu\text{m}$ (Figure S2c) and $14.75\ \mu\text{m}$ (Figure S2d). In other words, the AO-Fc was successfully prepared by amidoximation reaction of nitrile groups.

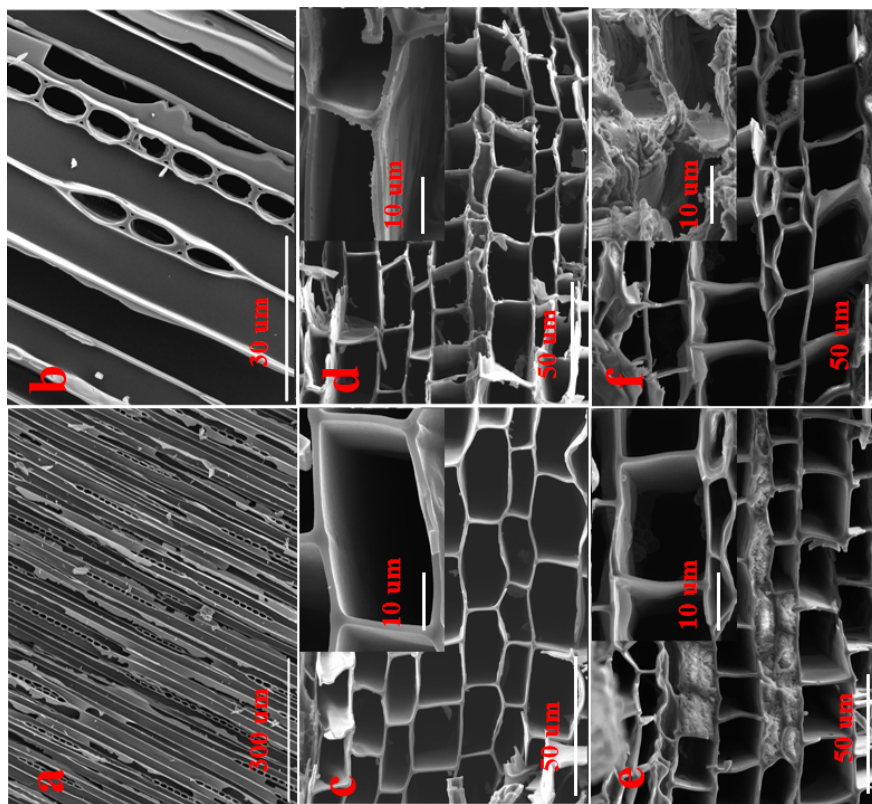


Figure 3 Vertical cross-section SEM images of Fc (a,b), and horizontal cross section SEM images of Fc (c), CN-Fc (c), CN-Fc1 (c) and AO-Fc(c)

Figure 4 showed dark-field images of CN-Fc, CN-Fc1 and AO-Fc with the corresponding elemental mapping. The images clearly showed the high number of nano precipitates as illustrated in corresponding Figure 4a-i and their elemental percentage was reported in Table 1. These precipitates were mostly C, N, and O

which are arranged in a rectangular homogenous pattern. The C and N elements of CN-Fc and CN-Fc1 were distributed in a rectangular fashion (Figure 4dgeh) confirming the presence of C and N elements in plenty and arranged in a homogenous pattern. Figure 4fi showed the presence of O in rectangular patterns confirmed the successful conversion of nitrile groups into amidoxime groups.

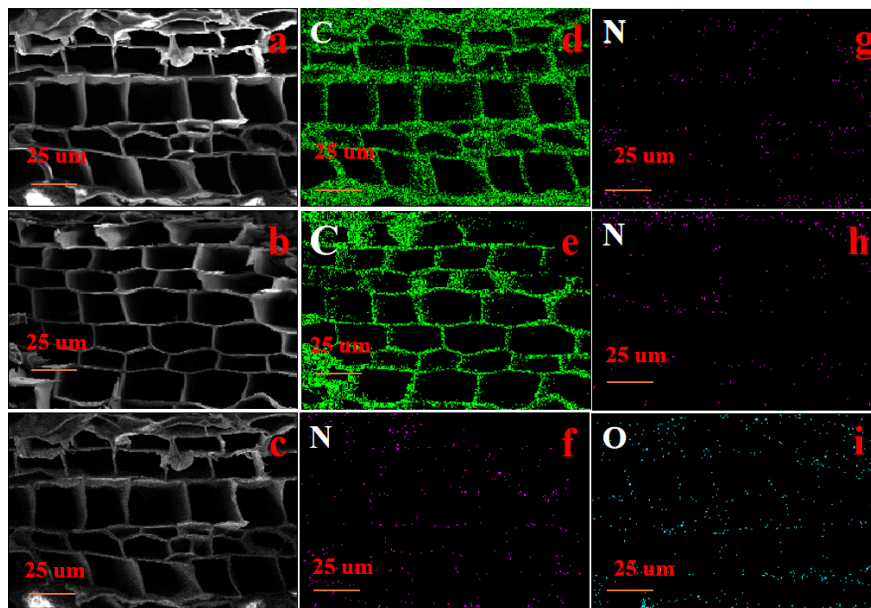


Figure 4 STEM+EDS maps of CN-Fc, CN-Fc1 and AO-Fc

The bet surface area, pore volume and pore size of Fc, CN-Fc, CN-Fc1 and AO-Fc were analyzed and the results were reported in Table 2. After functionalization of Fc, both surface area and pore volume were decreased from 155 m²/mg to 46 m²/mg and 0.07 cm³/g to 0.007 cm³/g (Figure 5), because of the large number of amidoxime groups occupying the pores space of Fc. Compared with amidoxime modified bamboo charcoal³⁶, AO-HNTs³⁹ and fiber⁴³ used for uranium extraction, the specific surface area of AO-Fc was relatively higher which might increase uranium adsorption capacity in seawater. The super-hydrophilicity of the material was determined by analyzing water contact angle measurements. The water contact angle of Fc and CN-Fc showed hydrophilicity and reached the water contact angle of 149° and 82.3° at the time of water contact with the adsorbent surface for 13 seconds (see video S1 and S2). On the other side, the water angle of AO-Fc reached 0° angle at a time gap of 0.02 seconds indicating AO-Fc possessed super-hydrophilicity due to the presence of enough hetero groups onto the surface of AO-Fc (see video S3).

Figure 5 Nitrogen adsorption and desorption isotherms (a) and distribution of pore size (b) of Fc, CN-Fc, CN-Fc1, and AO-Fc

Table 1 Weight percentage (%) by elemental analysis

Sample	Elements	Elements	Elements
	C %	N %	O %
Fc	100±0.80	-	-
CN-Fc	91 ±1.2	8.5±0.6	-
CN-Fc1	95.2±0.36	4.9±0.12	-
AO-Fc	57.3±0.36	28±1.54	14.7±0.86

Table 2 Nitrogen-adsorption desorption analysis of Fc, CN-Fc1, CN-Fc2 and AO-Fc

Sample	Pore size nm	Pore volume cm ³ /g	Surface area m ² /mg
Fc	1.3	0.07	155
CN-Fc	0.5	0.04	53
CN-Fc1	1.1	0.05	48
AO-Fc	0.4	0.005	46

3.2 Uranium recovery tests in simulate seawater

3.2.1 Analysis of optimal pH for uranium adsorption

It is well known the pH value of the adsorption solution markedly affects the uranium adsorption performance of the adsorbent due to the presence of different ionic charges present on the adsorbent surface and the uranium ions. Herein we study the effect of pH on uranium adsorption in the pH range of 3 to 10. From Figure 6a, as we have seen the adsorption capacity increased rapidly with increasing pH 3 to 8, at pH 8 the maximum adsorption capacity of AO-Fc was 411 ± 2 mg reported. With a further increase in pH, the adsorption capacity started to decrease. The optimum pH with maximum adsorption capacity of Fc, CN-Fc, and AO-Fc was 5, 6, and 8 confirmed the grafting of amidoxime groups adjusted the pKa value, resulting in shifting of pH to alkaline which is favorable for uranium under seawater conditions. The AO-Fc showed a positive shift towards an optimal pH of 8 towards the alkaline phase whereas the CN-Fc showed a small shift with an optimal pH of 6, confirming the role of amidoxime groups to shift the pKa of the base material. Further, NaCl showed no influence on uranium adsorption of AO-Fc, CN-Fc and Fc (Figure 6b) indicated a high concentration of NaCl in seawater would not affect uranium adsorption capacity of AO-Fc in seawater conditions.

Figure 6 Effect of solution pH (a) and various concentration of NaCl (b) on uranium adsorption capacity (mg/g)

3.2.2 Effect of contact time for uranium recovery capacity

To investigate the adsorption kinetics, the influence of contact on uranium adsorption onto adsorbent was analyzed for the contact time ranges of 5 to 450 min. As shown from Figure 7a, AO-Fc showed adsorption amount increasing rapidly from 5 to 80 min, indicating strong uranium adsorption from the initial uranium concentration solution. However, after 80 min the adsorption rate was decreased due to a decrease in diffusive resistance and active sites on the surface of AO-Fc during the adsorption process of uranium by amidoxime groups. After 350 min, there was no significant change in adsorption amount of AO-Fc, confirming the adsorption process achieved the equilibrium of adsorption at 350 min. CN-Fc and Fc showed lower adsorption capacity in comparison to AO-Fc due to the presence of low chelating sites and no significant adsorption capacity was increased after 150 min equilibrium of adsorption indicating equilibrium of adsorption was achieved. It is worth to report the longer equilibrium time and slower diffusion were attributed due to the low surface area and internal microporous structure of AO-Fc. To analyze the uranium adsorption mechanism, the adsorption kinetics of the adsorbent was studied by applying linear pseudo first order (LPFO) and pseudo second order kinetics (LPSO) and non-linear pseudo first order (NLPFO), and pseudo second order kinetics (NLPSO) (supporting information).

Both linear and non-linear plots of pseudo first order model and pseudo second order model and their kinetic parameters were shown in Figure 7b, Figure S3, Figure S4, Table 3 and Table S1. The kinetic parameters of linear plots of pseudo first order model and pseudo second order model were obtained by easily plotting a graph between $\ln(q_e - q_t)$ versus t and t/q_t versus t and the relevant parameters for studying the uranium adsorption were listed in Table 3 and Table S1. The kinetic parameters of non-linear plots of pseudo first order model and pseudo second order model were calculated by plotting a graph between q_t versus t and the relevant parameters were shown in Table S2. From the results of both linear and non-linear model fit (Table

3, Table S1 and Table S2), the correlation coefficient (R^2) of the pseudo second order model was close to unity than pseudo first order model, confirming the pseudo second order was better to discuss the adsorption behavior over entire adsorption process. The pseudo second kinetic model is based on the assumption that the rate-limiting step follows the chemisorption process through sharing valence electrons between uranium and the chelating site. Also, the validity of pseudo second order model fit was investigated by calculating p-value, q_{ecal} value (Figure S5) and statistical errors(supporting information), indicating the experimental data were best fitted with the pseudo second order. According to the theoretical calculation of Azizian et al. the adsorption experiment was carried out at a high initial concentration of solute >250 mg/L, the adsorption data were best fitted with pseudo first order rather than pseudo second order⁴⁴.

Figure 7 Adsorption kinetics of uranium onto AO-Fc, CN-Fc and Fc, the effect of contact time (a) and linear fitting by the pseudo second order (b) ($T = 303$ K and adsorbent dosage = 0.01 mg/L)

Table 3 Kinetic parameters for uranium obtained by linear regression.

Pseudo second order model

Adsorbent	K_2	q_{eexp}	q_{ecal}	R2	p-value	SSE	SAE	X^2	$\Delta q(\%)$
AO-Fc	0.00012±2E-05	410.000±0.004	400±10	0.996	9.6E-08	15.9	9.2	12.2	3.2
CN-Fc	0.00094±7E-05	30.00±0.01	29±1	0.996	1.1E-08	1.6	4.7	1.0	3.3
Fc	0.00124±0.0001	19.000±004	19±1	0.989	1.1E-07	1.2	10.0	1.8	3.5

3.2.3 Effect of equilibrium concentration on uranium recovery

To determine the adsorption capacity of AO-Fc, equilibrium adsorption studies were performed in a simulated uranium solution at different initial uranium concentrations. As shown in Figure 8a, the uranium adsorption amount increased rapidly with increasing the initial uranium concentration, but in due course, the adsorption capacity reached a plateau, which meant the adsorption capacity had reached the maximum adsorption capacity of the adsorbent. It was attributed, to more opportunities to adsorbent to intact with the higher uranium initial concentration until the maximum adsorption capacity was achieved. Further, the adsorption capacity of AO-Fc was higher than CN-Fc and Fc due to the presence of amidoxime groups. To measure the adsorption amount of adsorbent for uranium, various linear and non-linear isotherm models such as Langmuir isotherm model, Freundlich isotherm model, and Temkin isotherm model were applied to treat the experimental adsorption data at various uranium concentrations (Supporting information).

The fitting results of AO-Fc, CN-Fc and Fc were shown in Figure 8b, Figure S6 and Figure S7 and the values of various parameters are listed in Table 4 and Table S3 and Table S4. From results listed in Table 4 and Table S3 and Table S4, for AO-Fc the Langmuir isotherm model showed a higher regression coefficient ($R^2=0.998$) than Freundlich isotherm($R^2=0.944$) and Temkin isotherm ($R^2=0.985$), confirming the uranium adsorption onto the surface of AO-Fc followed a homogenous and monolayer adsorption coverage. Moreover, the applicability of the isotherm model was checked by calculating various statistical errors. For AO-Fc the Langmuir isotherm model showed lower error values as compared to Freundlich isotherm and Temkin isotherm, indicating the experimental data were best fitted with the Langmuir isotherm. Also, for AO-Fc the q_m (mg/g) calculated from the Langmuir isotherm model was 420 ± 12 mg/g at an equilibrium concentration of (0.5 mg/L), which was compared with the previously reported amidoxime adsorbents till now (Table 5). The results from Table 5 showed higher adsorption capacity for AO-Fc, indicating that it had greater potential to extract uranium from an aqueous solution.

Figure 8 Adsorption isotherm of uranium onto AO-Fc, CN-Fc and Fc, the effect of uranium initial concentration (a) and linear fitting by the Langmuir isotherm ($T=303$ K; adsorbent dosage = 0.01 mg/L and $t = 350$ min)

Table 4 Isothermmal parameters for uranium obtained by linear regression

	Langmuir isotherm model	Langmuir isotherm model	Langmuir isotherm model	Langmuir isotherm model	Langmuir isotherm model	Langmuir isotherm model	Langmuir isotherm model	Langmuir isotherm model	Langmuir isotherm model
Adsorbent	q_{eexp} (mg/g)	K_L (L/mg)	q_{ecal} (mg/g)	q_m (mg/g)	R^2	SSE	SAE	X^2	ΔC
AO-Fc	409±1	73.036380100±0.09	41.65±0.02	420±12	0.998	70	67	237	7
CN-Fc	30±1	10.280936±0.06	29.560±0.002	32.5±0.7	0.998	2	3	4	3
Fc	17±2	6.82781±0.05	16.330±0.004	19±2	0.999	2	1	4	3

3.3 Uranium recovery in seawater

To analyze the uranium adsorption capacity of AO-Fc in real seawater, adsorbent (7 mg) was added in a homemade adsorbent holder (syringe, Figure S1) and exposed to 20 L seawater and the complete homemade uranium adsorption set-up was shown in (Figure S1). The amount of uranium adsorbed from seawater was analyzed by knowing uranium concentration at different time intervals using (ICP-MS). For industrial applications, the adsorbent can be directly used to lower surface seawater for uranium extraction. The uranium adsorption kinetic results revealed that AO-Fc showed 6.60 mg/g adsorption capacity within one week, which was 75% of the total uranium adsorption. The maximum adsorption capacity reached 8.57 mg/g with 100 % adsorption efficiency after 11 days of the adsorption experiment (Figure 9ab). In comparison, AO-Fc showed efficient uranium adsorption from seawater (Table 5). Uranium adsorption capacity reflects the direct measurement of the amount of uranium adsorbed by an adsorbent and the distribution coefficient (K_d), determines the adsorbent affinity towards adsorbate. These results indicated that the adsorbent retaining high uranium adsorption capacity in presence of other coexisting ions might have a correspondingly higher K_d value than other coexisting ions in Figure 9c. Based on that, the evaluation of K_d (L/g) is an important parameter for choosing the most suitable adsorbent for further analysis.

Figure 9 Kinetics of uranium extraction (a,b) and distribution coefficient (K_d) of various ions in natural seawater (b)

Table 5 Comparison of various adsorbents for uranium extraction in seawater

Adorbent	Volume of seawater (L)/location	Adsorbent mass(mg/L)	Adsorption time(days)	Adsorption capacity
UiO-66-AO	1/Bohai Seawater	1	3	2.7
Anti-UiO-66	10	2	30	4.6
Anti-UiO-66	Simulated solution	-	-	2.84
UiO-66-3C4N	100/South China Sea	0.2	28	6.9
UiO-66-3C4N	Simulated solution	-	-	380.3
BP@CNF-MOF	100/ South China Sea	1	42	6.8
UiO-66-NH-(AO)	25/South China Sea	0.2	8	5.2
AOBCH	Simulated seawater	-	30	6.7
AO-Fc	20/South China Sea	0.35	11	8.6
AO-Fc	Simulated solution	-	0.236	409±1

3.4 Adsorbent stability and interaction with uranyl ions

The morphology of the adsorbent after uranium extraction/elution was analyzed by using SEM analysis. From Figure 10, we see the SEM images after uranium extraction (Figure 10a) and uranium elution (Figure 10b) confirmed that seawater exposed AO-Fc maintained the integrity of structure after reuse of several

cycles for a long time of seawater exposure. The detailed chemical composition of the uranium-loaded adsorbent (AO-Fc-U) adsorbent was analyzed by XPS and FTIR analysis and the results were compared with the adsorbent before uranium adsorption (AO-Fc) (Figure 11). The uranium-loaded adsorbent (AO-Fc-U) showed two peaks at 390.9 eV and 380.1 eV assigned to U 4f_{5/2} and U 4f_{7/2} confirmed the presence of uranium on AO-Fc (Figure 11a). As shown in Figure 11b, two types of Nitrogen peaks were observed at 400.05 eV and 398.4 eV assigned to N-H and C=N respectively. And also in accordance with Figure 11c, the binding energy of both N-H and C=N shifted to higher binding energy at 400.9 eV and 399.1 eV. To further analysis the uranium-loaded adsorbent was analyzed by FTIR. Compared with the results (Figure 11d), the uranium loaded spectra showed the shifts at various peaks or increase peak intensity. What is more, in the FTIR spectrum of AO-Fc, two new peaks were observed at 937 cm⁻¹ and 1161 cm⁻¹ confirming the presence of uranium on AO-Fc^{50,51}.

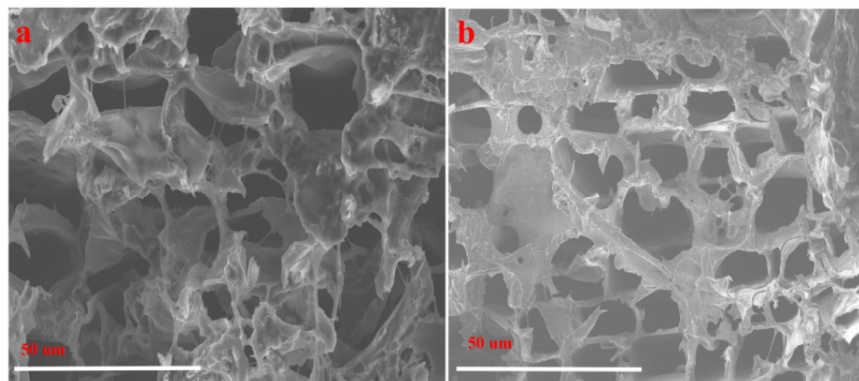


Figure 10 Uranium adsorbed AO-Fc exposed to natural seawater for 39 days (a) and uranium striped AO-Fc with elution solution Na₂CO₃ and H₂O₂ (b)

Figure 11 High-resolution XPS spectra of U 4f (a), N 1s before (b) and after uranium adsorption (c), and FTIR spectra (d)

3.5 Adsorbent regeneration and elution efficiency

Reusability is an important parameter for the industrial application of adsorbents that influences the cost of the adsorbent. For the reusability test, AO-Fc (7 mg) was used in 20 L seawater and the elution solution (1 M Na₂CO₃ and H₂O₂ 0.1 M) was fixed 3 mL per milligram of seawater exposed adsorbent. For uranium elution, the elution efficiency reached 99.9 % within 20 min, indicating the desired elution solution was better for uranium removal from AO-Fc (Figure 12a). The overall decrease in adsorption capacity and elution efficiency of AO-Fc were 1.8 % and 2 % up to seven cycles (Figure 12b,c), confirming the adsorbent can be used for several cycles, which would significantly decrease the uranium extraction cost. The decrease in adsorption capacity and elution efficiency might be due to the strong binding of uranyl ions with active functional groups. The adsorbent showed excellent structural stability and negligible loss of adsorbent (Figure S8) after seven adsorption-desorption cycles of AO-Fc (Figure 12b,c).

Figure 12 Elution efficiency of uranium in 1 M Na₂CO₃ and H₂O₂ 0.1 M (a), elution efficiency and uranium adsorption capacity of AO-Fc from natural seawater (b,c)

Conclusion

In conclusion, the new low-cost and facile prepared amidoxime modified adsorbent were analyzed qualitatively and quantitatively and can be considered as a potential adsorbent for uranium recovery from seawater. AO-Fc showed significant adsorption capacity and higher uranium selectivity, which is attributed due to amidoxime groups being present onto the surface of the 2D-open channel. In addition, the addition of amidoxime groups

not only enhanced the adsorption capacity and cracks the hydrophilicity but also adjusted the adsorbent pKa value.

The BET surface area of AO-Fc was lower as compared to Fc, indicating the surface area was not a grim factor for the adsorption mechanism. The uranium adsorption on AO-Fc was strongly dependent on pH value confirmed the adsorption was mainly occurred due to surface complexation.

The experimental adsorption simulation by various isotherm models exhibited that the R^2 value of Langmuir isotherm was close to unity obtained by linear regression. Also, the q_e calculated and the statistical analysis confirmed the adsorption data were best fitted with the Langmuir isotherm than other isotherm models.

Kinetic studies showed very fast uranium adsorption and the equilibrium of adsorption was achieved in 11 days, which was a lower contact time as compared to the adsorbents reported in Table 5 for uranium extraction from natural seawater.

The desorption and regeneration showed the adsorbent is economically and environmentally efficient. The higher adsorption capacity of AO-Fc towards uranium exhibits that the materials can be potential adsorbents for uranium extraction under seawater conditions.

Acknowledgments

This work was financially supported by the National Natural Science Foundation of China (No.21975206).

Conflict of interest

The authors declare no conflict of interest.

References

- [1] L. D. Loch, J. R. Gambino, W. H. Duckworth, *AIChE Journal* **1956** , 2 , DOI 10.1002/aic.690020213.
- [2] H. Zhang, W. Liu, A. Li, D. Zhang, X. Li, F. Zhai, L. Chen, L. Chen, Y. Wang, S. Wang, *Angewandte Chemie - International Edition* **2019** , 58 , DOI 10.1002/anie.201909718.
- [3] B. Aguila, Q. Sun, H. Cassady, C. W. Abney, B. Li, S. Ma, *ACS Applied Materials and Interfaces* **2019** , DOI 10.1021/acsami.9b09532.
- [4] R. Faizova, F. Fadaei-Tirani, R. Bernier-Latmani, M. Mazzanti, *Angewandte Chemie - International Edition* **2020** , 59 , DOI 10.1002/anie.201916334.
- [5] L. Feng, H. Wang, T. Feng, B. Yan, Q. Yu, J. Zhang, Z. Guo, Y. Yuan, C. Ma, T. Liu, N. Wang, *Angewandte Chemie* **2021** , DOI 10.1002/ange.202101015.
- [6] Y. Xie, C. Chen, X. Ren, X. Wang, H. Wang, X. Wang, *Progress in Materials Science* **2019** , 103 , DOI 10.1016/j.pmatsci.2019.01.005.
- [7] Y. Wang, Y. Zhang, Q. Li, Y. Li, L. Cao, W. Li, *Carbohydrate Polymers* **2020** , 245 , DOI 10.1016/j.carbpol.2020.116627.
- [8] D. S. Sholl, R. P. Lively, *Nature* **2016** , 532 , DOI 10.1038/532435a.
- [9] F. Yu, Z. Zhu, S. Wang, Y. Peng, Z. Xu, Y. Tao, J. Xiong, Q. Fan, F. Luo, *Chemical Engineering Journal* **2021** , 412 , DOI 10.1016/j.cej.2020.127558.
- [10] S. Doudou, K. Arumugam, D. J. Vaughan, F. R. Livens, N. A. Burton, in *Physical Chemistry Chemical Physics* , **2011** .
- [11] M. F. Byers, E. Schneider, *Industrial and Engineering Chemistry Research* **2015** , 55 , DOI 10.1021/acs.iecr.5b03242.
- [12] G. A. Gill, L. J. Kuo, C. J. Janke, J. Park, R. T. Jeters, G. T. Bonheyo, H. Bin Pan, C. Wai, T. Khangaonkar, L. Bianucci, J. R. Wood, M. G. Warner, S. Peterson, D. G. Abrecht, R. T. Mayes,

- C. Tsouris, Y. Oyola, J. E. Strivens, N. J. Schlafer, R. S. Addleman, W. Chouyyok, S. Das, J. Kim, K. Buesseler, C. Breier, E. D'Alessandro, *Industrial and Engineering Chemistry Research* **2016** , DOI 10.1021/acs.iecr.5b03649.
- [13] F. Endrizzi, L. Rao, *Chemistry - A European Journal***2014** , *20* , DOI 10.1002/chem.201403262.
- [14] Z. Bai, Q. Liu, H. Zhang, J. Yu, R. Chen, J. Liu, D. Song, R. Li, J. Wang, *ACS Applied Materials and Interfaces* **2020** , *12* , DOI 10.1021/acsami.0c03007.
- [15] Q. Sun, B. Aguila, J. Perman, A. S. Ivanov, V. S. Bryantsev, L. D. Earl, C. W. Abney, L. Wojtas, S. Ma, *Nature Communications***2018** , *9* , DOI 10.1038/s41467-018-04032-y.
- [16] Q. Sun, L. Zhu, B. Aguila, P. K. Thallapally, C. Xu, J. Chen, S. Wang, D. Rogers, S. Ma, *Nature Communications* **2019** , *10* , DOI 10.1038/s41467-019-09630-y.
- [17] R. Wen, Y. Li, M. Zhang, X. Guo, X. Li, X. Li, J. Han, S. Hu, W. Tan, L. Ma, S. Li, *Journal of Hazardous Materials***2018** , *358* , DOI 10.1016/j.jhazmat.2018.06.059.
- [18] Q. Sun, B. Aguila, L. D. Earl, C. W. Abney, L. Wojtas, P. K. Thallapally, S. Ma, *Advanced Materials* **2018** , *30* , DOI 10.1002/adma.201705479.
- [19] C.-P. Niu, C.-R. Zhang, W.-R. Cui, S.-M. Yi, R.-P. Liang, J.-D. Qiu, *Journal of Hazardous Materials* **2022** , *425* , DOI 10.1016/j.jhazmat.2021.127951.
- [20] Y. Yuan, Q. Meng, M. Faheem, Y. Yang, Z. Li, Z. Wang, D. Deng, F. Sun, H. He, Y. Huang, H. Sha, G. Zhu, *ACS Central Science***2019** , *5* , DOI 10.1021/acscentsci.9b00494.
- [21] W. Liu, X. Dai, Z. Bai, Y. Wang, Z. Yang, L. Zhang, L. Xu, L. Chen, Y. Li, D. Gui, J. Diwu, J. Wang, R. Zhou, Z. Chai, S. Wang, *Environmental Science and Technology* **2017** , *51* , DOI 10.1021/acs.est.6b06305.
- [22] T. Zheng, Z. Yang, D. Gui, Z. Liu, X. Wang, X. Dai, S. Liu, L. Zhang, Y. Gao, L. Chen, D. Sheng, Y. Wang, J. Diwu, J. Wang, R. Zhou, Z. Chai, T. E. Albrecht-Schmitt, S. Wang, *Nature Communications***2017** , *8* , DOI 10.1038/ncomms15369.
- [23] M. Monier, D. A. Abdel-Latif, H. A. Mohammed, *International Journal of Biological Macromolecules* **2015** , DOI 10.1016/j.ijbiomac.2014.12.001.
- [24] M. Monier, D. A. Abdel-Latif, *Carbohydrate Polymers***2013** , DOI 10.1016/j.carbpol.2013.05.062.
- [25] M. Z. C. Hu, M. Reeves, *AIChE Journal* **1999** , *45* , DOI 10.1002/aic.690451109.
- [26] K. Tian, J. Wu, J. Wang, *Radiochimica Acta***2018** , *106* , DOI 10.1515/ract-2017-2913.
- [27] Z. Zhang, Z. Dong, Y. Dai, S. Xiao, X. Cao, Y. Liu, W. Guo, M. Luo, Z. Le, *RSC Advances* **2016** , *6* , DOI 10.1039/c6ra21986a.
- [28] P. Zhang, L. Wang, Z. Huang, J. Yu, Z. Li, H. Deng, T. Yin, L. Yuan, J. K. Gibson, L. Mei, L. Zheng, H. Wang, Z. Chai, W. Shi, *ACS Applied Materials and Interfaces* **2020** , *12* , DOI 10.1021/acsami.0c00861.
- [29] X. Xu, L. Xu, J. Ao, Y. Liang, C. Li, Y. Wang, C. Huang, F. Ye, Q. Li, X. Guo, J. Li, H. Wang, S. Ma, H. Ma, *Journal of Materials Chemistry A* **2020** , *8* , DOI 10.1039/d0ta07180c.
- [30] C. Zhang, X. Cai, W. Chen, S. Yang, D. Xu, Y. Fang, X. Yu, *ACS Sustainable Chemistry and Engineering* **2018** , *6* , DOI 10.1021/acssuschemeng.8b01189.
- [31] M. Mousa, Y. Dong, *ACS Sustainable Chemistry and Engineering* **2018** , *6* , DOI 10.1021/acssuschemeng.7b02750.
- [32] V. Kumar, P. K. Tyagi, *Journal of Alloys and Compounds***2018** , *767* , DOI 10.1016/j.jallcom.2018.06.123.

- [33] K. Saito, K. Uezu, T. Hori, S. Furusaki, T. Sugo, J. Okamoto, *AIChE Journal* **1988** , *34* , DOI 10.1002/aic.690340308.
- [34] X. Zhou, L. Shi, T. B. Moghaddam, M. Chen, S. Wu, X. Yuan, *Journal of Hazardous Materials* **2022** , *425* , DOI 10.1016/j.jhazmat.2021.128003.
- [35] J. Liao, L. Ding, Y. Zhang, W. Zhu, *Journal of Hazardous Materials* **2022** , *423* , DOI 10.1016/j.jhazmat.2021.127190.
- [36] Y. Wang, Z. Lin, H. Zhang, Q. Liu, J. Yu, J. Liu, R. Chen, J. Zhu, J. Wang, *Journal of Colloid and Interface Science* **2021** , *598* , DOI 10.1016/j.jcis.2021.03.154.
- [37] Z. Guo, T. Pereira, O. Choi, Y. Wang, H. T. Hahn, *Journal of Materials Chemistry* **2006** , *16* , DOI 10.1039/b603020c.
- [38] A. O. Alhareb, H. B. M. Akil, Z. A. B. Ahmad, *Journal of Thermoplastic Composite Materials* **2017** , *30* , DOI 10.1177/0892705715616856.
- [39] S. Zhao, Y. Yuan, Q. Yu, B. Niu, J. Liao, Z. Guo, N. Wang, *Angewandte Chemie - International Edition* **2019** , *58* , DOI 10.1002/anie.201908762.
- [40] S. Shi, Y. Qian, P. Mei, Y. Yuan, N. Jia, M. Dong, J. Fan, Z. Guo, N. Wang, *Nano Energy* **2020** , *71* , DOI 10.1016/j.nanoen.2020.104629.
- [41] D. Sun, X. Hao, X. Chen, X. Huang, *Wood and Fiber Science* **2015** , *47* .
- [42] C. H. Chia, S. D. Joseph, A. Rawal, R. Linser, J. M. Hook, P. Munroe, *Journal of Analytical and Applied Pyrolysis* **2014** , *109* , DOI 10.1016/j.jaap.2014.06.009.
- [43] X. Xu, H. Zhang, J. Ao, L. Xu, X. Liu, X. Guo, J. Li, L. Zhang, Q. Li, X. Zhao, B. Ye, D. Wang, F. Shen, H. Ma, *Energy and Environmental Science* **2019** , *12* , DOI 10.1039/c9ee00626e.
- [44] S. Azizian, *Journal of Colloid and Interface Science* **2004** , *276* , DOI 10.1016/j.jcis.2004.03.048.
- [45] L. Chen, Z. Bai, L. Zhu, L. Zhang, Y. Cai, Y. Li, W. Liu, Y. Wang, L. Chen, J. Diwu, J. Wang, Z. Chai, S. Wang, *ACS Applied Materials and Interfaces* **2017** , *9* , DOI 10.1021/acsami.7b12396.
- [46] Q. Yu, Y. Yuan, J. Wen, X. Zhao, S. Zhao, D. Wang, C. Li, X. Wang, N. Wang, *Advanced Science* **2019** , DOI 10.1002/advs.201900002.
- [47] Y. Yuan, S. Feng, L. Feng, Q. Yu, T. Liu, N. Wang, *Angewandte Chemie - International Edition* **2020** , DOI 10.1002/anie.201916450.
- [48] M. Chen, T. Liu, X. Zhang, R. Zhang, S. Tang, Y. Yuan, Z. Xie, Y. Liu, H. Wang, K. V. Fedorovich, N. Wang, *Advanced Functional Materials* **2021** , *31* , 1–10.
- [49] L. Ma, J. Gao, C. Huang, X. Xu, L. Xu, R. Ding, H. Bao, Z. Wang, G. Xu, Q. Li, P. Deng, H. Ma, *ACS Applied Materials & Interfaces* **2021** , DOI 10.1021/acsami.1c18625.
- [50] C. Zhao, J. Liu, Y. Deng, Y. Tian, G. Zhang, J. Liao, J. Yang, Y. Yang, N. Liu, Q. Sun, *Journal of Cleaner Production* **2019** , *236* , DOI 10.1016/j.jclepro.2019.117624.
- [51] A. S. El-Sheikh, E. A. Haggag, N. R. A. El-Rahman, *Radiochemistry* **2020** , *62* , DOI 10.1134/S1066362220040074.

Hosted file

Graphical Abstract.docx available at <https://authorea.com/users/472295/articles/563229-a-novel-preparation-and-vapour-phase-modification-of-2d-open-channel-bio-adsorbent-via-atrp-for-uranium-separation>